



# Novel D- $\pi$ -A system based on zinc porphyrin dyes for dye-sensitized solar cells: Synthesis, electrochemical, and photovoltaic properties

Kang Deuk Seo<sup>a</sup>, Myung Jun Lee<sup>a</sup>, Hae Min Song<sup>a</sup>, Hong Seok Kang<sup>b</sup>, Hwan Kyu Kim<sup>a,\*</sup>

<sup>a</sup> Department of Advanced Materials Chemistry & Centre for Advanced Photovoltaic Materials (ITRC), Korea University, ChungNam 339-700, Republic of Korea

<sup>b</sup> Department of Nano & Advanced Materials, College of Engineering, Jeonju University, Hyoja-dong, Chonju, Chonbuk 560-759, Republic of Korea

## ARTICLE INFO

### Article history:

Received 17 November 2011

Received in revised form

13 December 2011

Accepted 15 December 2011

Available online 27 December 2011

### Keywords:

Porphyrin

Triphenylamine electron-donating group

D- $\pi$ -A system

Dye-sensitized solar cell

Charge recombination

Short-circuit photocurrent density

## ABSTRACT

We have designed and synthesized novel zinc porphyrin dyes which have a D- $\pi$ -A system based on porphyrin derivatives containing a triphenylamine (TPA) electron-donating group and a phenyl carboxyl anchoring group substituted at the meso position of the porphyrin ring, yielding the push-pull porphyrins as the most efficient green dye for dye-sensitized solar cell (DSSC) applications. The synthesis and characterization of a novel D- $\pi$ -A system based on zinc-porphyrin derivatives have been investigated through their photophysical and photoelectrochemical studies. A large red-shift of the absorption maxima due to introduction of the TPA moiety at the meso position of the porphyrin ring was expected in the D- $\pi$ -A porphyrins, but the absorption maxima of **HKK-Por** dyes were a little red-shifted in contrast to Zn[5,-10,15-triphenyl-20-(4-carboxylphenyl)-porphyrin], due to the tilted structure between TPA and the porphyrin unit. Under the photovoltaic performance measurement, the maximum incident photon-to-current conversion efficiency (IPCE) value of the DSSC based on **HKK-Por 5** was slightly higher than the efficiencies of the DSSCs based on other **HKK-Por** dyes due to the introduction of the alkoxy group into the TPA moiety at the meso position of the porphyrin ring. A maximum photon-to-electron conversion efficiency of 3.36% was achieved with the DSSC based on **HKK-Por 5** dye ( $J_{SC} = 9.04 \text{ mA/cm}^2$ ,  $V_{OC} = 0.57 \text{ V}$ ,  $FF = 0.66$ ) under AM1.5 irradiation ( $100 \text{ mWcm}^{-2}$ ).

© 2011 Elsevier Ltd. All rights reserved.

## 1. Introduction

The ever increasing consumption of fossil fuels, causing global warming and environmental pollution, has led to a greater focus on renewable energy sources and sustainable development. Dye-sensitized solar cells (DSSCs) have attracted considerable attention in recent years [1]. DSSCs based on mesoporous nanocrystalline TiO<sub>2</sub> films have attracted significant attention due to their low cost and high sunlight-to-electric power conversion efficiencies of 10–12% [2–10]. In recent years, interest in metal-free organic dyes as an alternative to noble metal complexes has increased due to their many advantages, such as diversity of molecular structures, high molar extinction coefficient, and simple synthesis as well as low cost and environmental benefits [11,12].

Porphyrins are one of the most widely studied sensitizers for DSSCs because of their strong Soret (400–450 nm) and moderate Q bands (550–600 nm) [13–20]. The porphyrin-based dyes have several intrinsic advantages, such as the good photostability offered

by the natural chlorophylls, their rigid molecular structures with large absorption coefficients in the visible region, and their many reaction sites, that is, four meso and eight beta positions, available for functionalization. Fine tuning of their optical, physical, and electrochemical properties thus becomes feasible [21–28]. In addition, a high  $\eta$  value of porphyrin dye of up to 10.2% in full sunlight has been achieved by Eric Diau and co-workers [29]. To further design and develop the more efficient porphyrin dyes for DSSCs, the predominant light-harvesting abilities of dyes in visible and near-IR light are important to get a larger photocurrent response.

In our previous report [30], porphyrin with a carbazole-containing triphenylamine (TPA) moiety and a mesityl group introduced at the 5, 20 position was designed and synthesized. Here, we have designed and synthesized novel zinc porphyrin dyes that have a D- $\pi$ -A system based on porphyrin derivatives containing a TPA electron-donating group and a meso-substituted phenyl carboxyl anchoring group attached at the meso position of the porphyrin ring. To increase the electron-donating ability of the D- $\pi$ -A system based on porphyrin derivatives, to decrease the dye aggregation, a hexyloxy substituent was introduced into the TPA moiety. Furthermore to decrease the rotation of the phenyl unit,

\* Corresponding author. Tel.: +82 41 860 1493; fax: +82 41 867 5396.

E-mail address: [hkk777@korea.ac.kr](mailto:hkk777@korea.ac.kr) (H.K. Kim).

a mesityl group was introduced at the 5, 20 position of the **HKK-Por 4** and **HKK-Por 5**, yielding the push-pull porphyrins as the most efficient green dye for DSSC applications.

## 2. Experimental

### 2.1. Materials

Pyrrole, benzaldehyde, trifluoroacetic acid, 2,4,6-trimethylbenzaldehyde, TPA, copper iodide, 18-crown-6, 4-iodophenol, 3-bromomethyl-heptane, aniline, potassium carbonate, triethylamine, zinc acetate dihydrate, 1,2-dichlorobenzene, acetic acid, methyl 4-formylbenzoate, sodium hydride, and potassium hydride were used as received from Sigma–Aldrich without further purification. Chloroform, toluene, dichloromethane, n-hexane, ethanol, tetrahydrofuran, methanol, N,N-dimethylformamide, hydrochloric acid, ether, and anhydrous potassium carbonate were purchased from Samchun Co. 1,2-Dichloroethane was purchased from TCI Co.

### 2.2. Measurement

The  $^1\text{H}$  NMR spectra were recorded at room temperature with Varian Oxford 300 spectrometers and chemical shifts were reported in parts per million (ppm) with tetramethylsilane as an internal standard. FT-IR spectra were measured on KBr pellets with a Perkin Elmer Spectrometer. UV–visible absorption spectra were obtained in THF on a Shimadzu UV-2401PC spectrophotometer. Cyclic voltammetry was carried out with a Versa STAT3 (AMETEK). A three-electrode system was used, consisted of a reference electrode (Ag/AgCl), a working electrode, and a platinum wire electrode. The redox potential of dyes on  $\text{TiO}_2$  was measured in  $\text{CH}_3\text{CN}$  with 0.1 M TBAPF<sub>6</sub> with a scan rate of  $50 \text{ mV s}^{-1}$ .

### 2.3. Density functional theory (DFT)/time-dependent DFT (TD-DFT) calculations

Structural optimization of **HKK-Por** dyes was done with a PBE exchange-correlation function using the Vienna ab initio simulation package (VASP) [31,32]. We used 400 eV as the cut-off energy, and the conjugate gradient method was employed to optimize the geometry until the force exerted on an atom was less than  $0.03 \text{ eV/\text{Å}}$ . In order to calculate the absorption spectra, we performed the TD-DFT calculations in the gas phase using the 6-31G(d) basis set in GAUSSIAN03 program [33]. We focused on transitions occurring in the range of 350–800 nm, specifically those whose oscillation strengths were greater than 0.1.

### 2.4. Synthesis

#### 2.4.1. 5-Phenyl dipyrromethane (**1**)

A solution of benzaldehyde (1 mmol) in 3 ml pyrrole (43 mmol) with a catalytic amount of trifluoroacetic acid (0.1 mmol) was vigorously stirred at room temperature for 15 min. The crude product is obtained by dilution with  $\text{CH}_2\text{Cl}_2$ , washing with dilute NaOH, and concentration of the organic layer. The excess pyrrole is recovered by vacuum distillation at room temperature. Column chromatography on silica of the resulting brownish solid affords the white 5-phenyl dipyrromethane in 29% yield.  $^1\text{H}$  NMR ( $\text{CDCl}_3$ )  $\delta$  (TMS, ppm): 7.21–7.34 (m, 5H), 6.70 (q, 2H), 6.17 (q, 2H), 5.93 (s, 2H), 5.48 (s, 1H).

#### 2.4.2. 5-Mesityl dipyrromethane (**2**)

A solution of 2,4,6-trimethylbenzaldehyde (2.65 ml, 18 mmol) and pyrrole (50 ml, 720 mmol) was degassed by argon bubbling for 15 min. Trifluoroacetic acid (0.14 ml, 1.8 mmol) was then added and

the solution was stirred under argon at room temperature for an additional hour and then quenched with triethylamine (0.4 ml). The mixture was diluted with toluene (150 ml), washed with brine, and then dried with  $\text{MgSO}_4$ . The solvent was removed under reduced pressure and then the unreacted pyrrole was removed by vacuum distillation at room temperature. The residue was dissolved in  $\text{CH}_2\text{Cl}_2$  and filtered through a short pad of silica using  $\text{CH}_2\text{Cl}_2$  as the eluent. Evaporation of the solvent under reduced pressure resulted in a brown solid. This solid was washed with cyclohexane and then with hexane, giving a pale yellow solid, which was collected by filtration (yield: 70%).  $^1\text{H}$  NMR ( $\text{CDCl}_3$ )  $\delta$  (TMS, ppm): 7.95 (s, 2H), 6.87 (s, 2H), 6.67 (s, 2H), 6.18 (m, 2H), 6.02 (s, 2H), 5.93 (s, 1H), 2.27 (s, 3H), 2.06 (s, 6H).

#### 2.4.3. 4-Formyl triphenylamine (**3**)

$\text{POCl}_3$  (4.47 ml, 48.67 mmol) was added dropwise to 8.5 ml DMF with stirring under dry conditions, and the temperature was kept below  $10^\circ\text{C}$ . After adding a mixture of TPA (5.97 g, 24.34 mmol) and 2 ml DMF to the reaction vessel at this temperature, the reaction mixture was maintained at  $35^\circ\text{C}$  for 24 h. Subsequently, the reaction solution was poured into ice water and the precipitated mixture was filtered and washed with water. The crude product was purified by column chromatography (silica gel, dichloromethane) to afford a yellow solid (yield: 83%).  $^1\text{H}$  NMR ( $\text{CDCl}_3$ )  $\delta$  (TMS, ppm): 9.81 (s, 1H), 7.68 (d, 2H), 7.36–7.31 (m, 4H), 7.19–7.14 (m, 6H), 7.02 (d, 2H).

#### 2.4.4. 1-(2-Ethylhexyloxy)-4-iodobenzene (**4**)

4-Iodophenol (10 g, 10 mmol) was dissolved in 200 ml of DMF, and then  $\text{K}_2\text{CO}_3$  (9.42 g, 68.18 mmol) was added. The mixture was stirred in a  $\text{N}_2$  atmosphere at  $60^\circ\text{C}$ . After 30 min, 2-ethylhexylbromide (9.70 ml, 54.54 mmol) was dissolved in 50 ml of DMF and added to the flask dropwise. The reaction was continued for 48 h.  $\text{K}_2\text{CO}_3$  was filtered out, the solvent was evaporated, and then the crude product was washed with water and dried with  $\text{MgSO}_4$ . The pure white liquid product was obtained by silica column chromatography (eluent: hexane) (yield: 77%).  $^1\text{H}$  NMR ( $\text{CDCl}_3$ )  $\delta$  (TMS, ppm): 7.54 (d, 2H), 6.69 (d, 2H), 3.81 (d, 2H), 1.17–1.75 (m, 1H), 1.36–1.55 (m, 8H), 0.95 (t, 6H).

#### 2.4.5. Bis-[4-(2-ethylhexyloxy)-phenyl]-phenylamine (**5**)

Aniline (1.78 g, 19.5 mmol), 1-(2-ethylhexyloxy)-4-iodobenzene (14.4 g, 43.3 mmol) (5 g, 15.05 mmol), copper(I) iodide (4.83 g, 76.0 mmol), 1,10-phenanthroline (0.05 g, 0.3 mmol), and potassium hydroxide flakes (2.96 g, 52.7 mmol) were dissolved in 1,2-dichlorobenzene (50 ml). The reaction mixture was rapidly heated over a period of 30 min to  $125^\circ\text{C}$  and maintained at this temperature for 24 h. After cooling, the mixture was diluted with dichloromethane and washed with 1 N HCl and brine before being dried over  $\text{MgSO}_4$ . The crude product was purified by column chromatography to give the product (yield: 80%) as colourless oil.  $^1\text{H}$  NMR ( $\text{CDCl}_3$ )  $\delta$  (TMS, ppm): 7.46 (d, 2H), 7.17 (m, 1H), 7.03 (d, 4H), 6.90 (d, 2H), 6.85 (d, 4H), 3.81 (d, 4H), 1.17–1.75 (m, 2H), 1.36–1.55 (m, 16H), 0.95 (t, 12H).

#### 2.4.6. 4-{Bis-[4-(2-ethylhexyloxy)-phenyl]-amino}-benzaldehyde (**6**)

$\text{POCl}_3$  (0.73 ml, 7.8 mmol) was slowly added to a stirred solution of bis-[4-(2-ethylhexyloxy)-phenyl]-phenylamine (3.78 g, 7.67 mmol) and dimethylformamide (0.6 ml, 7.8 mmol) in 50 ml of 1,2-dichloroethane. Subsequently the solution was refluxed for 2 h, cooled, and poured into water. The resulting mixture was extracted with dichloromethane. After drying with  $\text{MgSO}_4$ , the solvent together with the 1,2-dichloroethane and DMF was removed by evaporation under reduced pressure. The crude product was purified by silica gel column chromatography to give a product (yield:

78%) as colourless oil.  $^1\text{H NMR}$  ( $\text{CDCl}_3$ )  $\delta$  (TMS, ppm): 9.92 (s, 1H), 7.57 (d, 2H), 7.09 (d, 4H), 6.85 (d, 2H), 6.79 (d, 4H), 3.81 (d, 4H), 1.71–1.75 (m, 2H), 1.36–1.55 (m, 16H), 0.95 (t, 12H).

#### 2.4.7. 5,15-Bisphenyl-15-triphenylamino(4-methoxycarbonylphenyl) porphyrin (7)

The mixture of methyl-4-formylbenzoate (0.67 g, 4.05 mmol), 4-formyltriphenyl amine (1.1 g, 4.05 mmol), and 5-phenyldipyrromethane (1.8 g, 8.10 mmol) was condensed in dichloromethane (2.41 L) with TFA (0.4 ml, 5.10 mmol) at room temperature for 1 h. Then DDQ (2.35 g, 10.4 mmol) was added, after which the mixture was stirred for 1 h at room temperature. Next TEA (3 ml) was added, and the mixture was stirred for 1 h at room temperature. The solvent was removed under reduced pressure. The residue was then dissolved in  $\text{CHCl}_3$  and passed through a short silica gel column. This mixture was purified with a second column to afford the compound FB-por (yield: 3%).  $^1\text{H NMR}$  ( $\text{CDCl}_3$ )  $\delta$  (TMS, ppm): 9.01 (d, 2H), 8.88 (d, 2H), 8.85 (d, 2H), 8.78 (d, 2H), 8.44 (d, 2H), 8.31 (d, 2H), 8.22 (d, 4H), 8.07 (d, 2H), 7.77 (d, 6H), 7.40–7.46 (m, 10H), 7.14 (d, 2H), 4.11 (s, 3H),  $-2.74$  (s, 2H); FT-IR (KBr pellet,  $\text{cm}^{-1}$ ): 1720 (ester, C=O), 3455 (amine,  $-\text{NH}$ ).

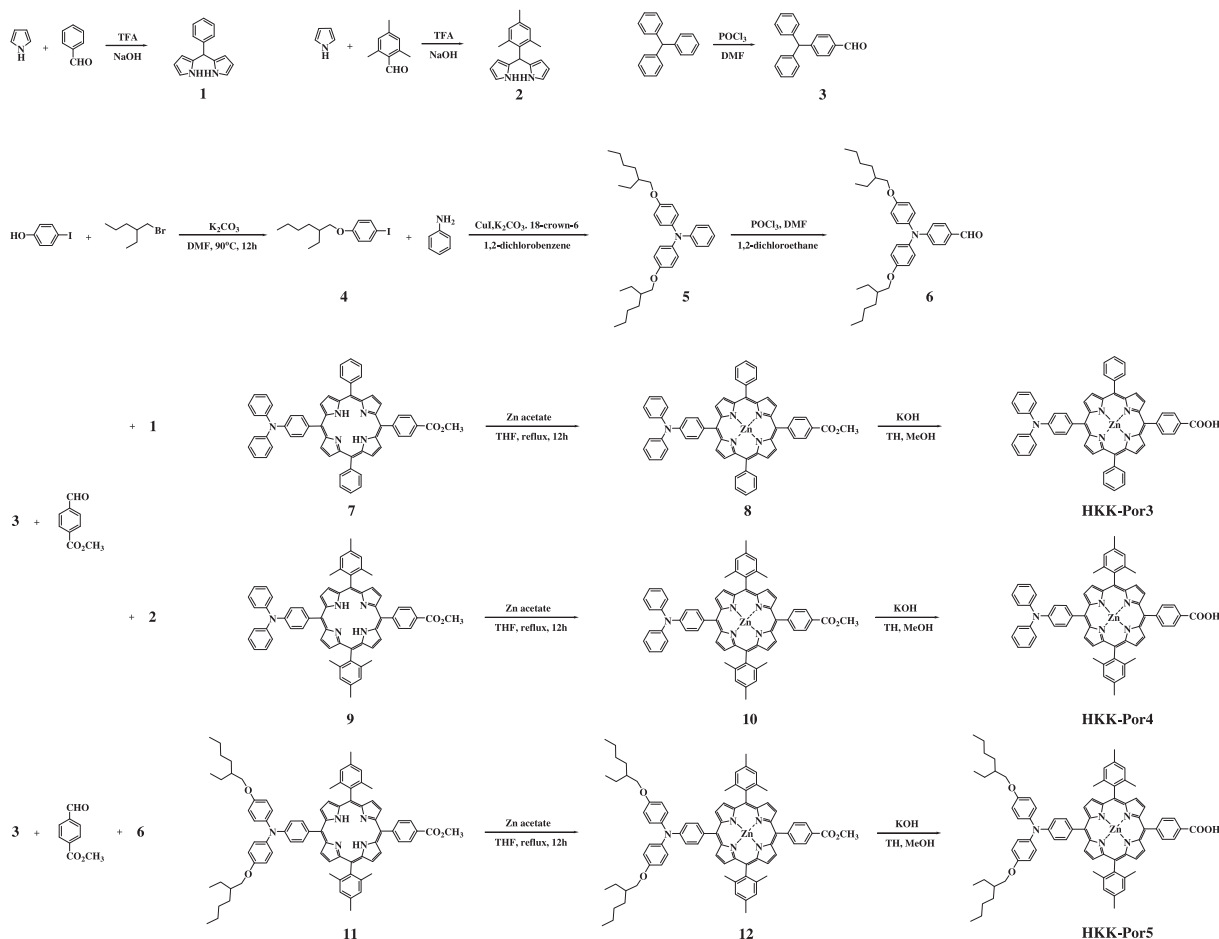
#### 2.4.8. 5,15-Bisphenyl-15-triphenylamino(4-methoxycarbonylphenyl) porphyrinatozinc (8)

5,15-Bisphenyl-15-triphenylamino(4-methoxycarbonylphenyl) porphyrin (0.15 g, 0.18 mmol) and zinc acetate dehydrate (0.2 g, 0.89 mmol) were suspended in dry THF (20 ml). The mixture was

then purged with  $\text{N}_2$  and slowly heated to  $80^\circ\text{C}$ . It was then brought to reflux under  $\text{N}_2$  until there was no free base left as revealed by TLC (24 h). The mixture was then cooled to room temperature and the solvent was removed by vacuum distillation. The crude product left behind was then dried completely and purified with a column to afford the compound Zn-por (yield: 86%).  $^1\text{H NMR}$  ( $\text{CDCl}_3$ )  $\delta$  (TMS, ppm): 9.01 (d, 2H), 8.85 (d, 2H), 8.88 (d, 2H), 8.78 (d, 2H), 8.44 (d, 2H), 8.31 (d, 2H), 8.22 (d, 4H), 8.07 (d, 2H), 7.77 (d, 6H), 7.40–7.46 (m, 10H), 7.14 (d, 2H), 4.11 (s, 3H); FT-IR (KBr pellet,  $\text{cm}^{-1}$ ): 1720 (ester, C=O).

#### 2.4.9. 5,15-Bisphenyl-15-triphenylamino(4-carboxyphenyl)porphyrinatozinc (HKK-Por 3)

5,15-Bisphenyl-15-triphenylamino(4-methoxycarbonylphenyl) porphyrinatozinc (0.1 g, 0.12 mmol) and KOH (0.08 g, 0.14 mmol) were dissolved in THF–EtOH– $\text{H}_2\text{O}$  (1:1:0.1, 50 ml), and the solution was refluxed for 12 h. The mixture was then cooled to room temperature, acidified with concentrated HCl, and extracted with  $\text{CH}_2\text{Cl}_2$ . The organic phase was washed with sodium bicarbonate solution and water and dried with  $\text{MgSO}_4$ . The crude product left behind was then dried completely and purified with a column to afford the compound Zn-por-COOH (yield: 68%).  $^1\text{H NMR}$  ( $\text{CDCl}_3$ )  $\delta$  (TMS, ppm): 9.01 (d, 2H), 8.85 (d, 2H), 8.88 (d, 2H), 8.78 (d, 2H), 8.44 (d, 2H), 8.31 (d, 2H), 8.22 (d, 4H), 8.07 (d, 2H), 7.77 (d, 6H), 7.40–7.46 (m, 10H), 7.14 (d, 2H);  $\lambda_{\text{max,abs}}$  in THF: 424.5, 556.5, 598.5.  $\lambda_{\text{max,em}}$  in THF: 608.9, 659.1; FT-IR (KBr pellet,  $\text{cm}^{-1}$ ): 2400–3400 (carboxylic acid,  $-\text{COOH}$ ); FAB-MS ( $m/z$ ): calcd. 887.2, found 888.0.



Scheme 1. Chemical structures and synthesis of HKK-Por dyes.

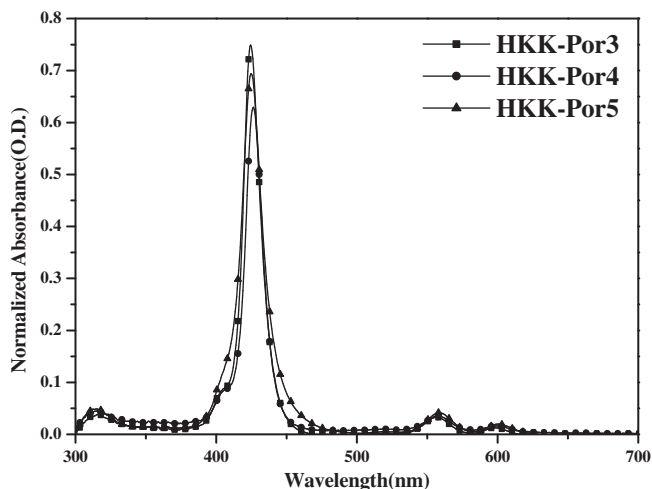


Fig. 1. Absorption spectra of **HKK-Por** dyes in THF solvent ( $1.0 \times 10^{-4}$  M).

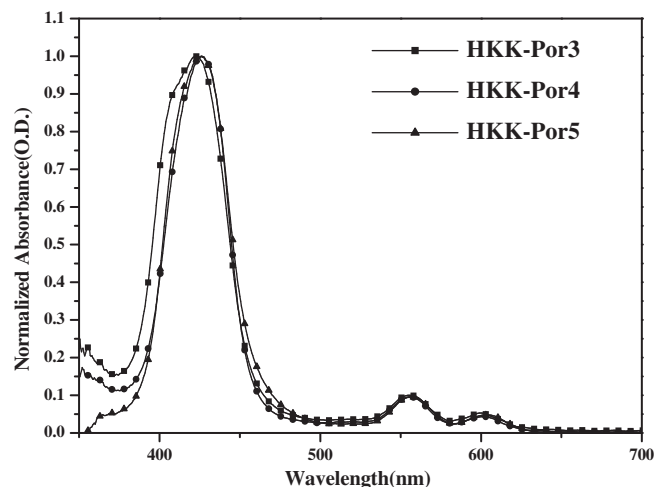


Fig. 2. Absorption spectra of **HKK-Por** dyes on  $\text{TiO}_2$  film.

#### 2.4.10. 5,15-Bis(2,4,6-trimethylphenyl)-15-triphenylamino(4-methoxycarbonylphenyl) porphyrin (**9**)

Methyl-4-formylbenzoate (0.56 g), 4-formyl triphenylamine (0.9 g), and 5-mesityl dipyrromethane (1.8 g) were condensed in dichloromethane (2.4 L) with TFA (0.8 ml) at room temperature for 1 h. DDQ (1.98 g) was added, and the mixture was stirred for 1 h at room temperature. Then TEA (3 ml) was added, after which the mixture was stirred for 1 h at room temperature. The solvent was removed under reduced pressure. The residue was then dissolved in  $\text{CHCl}_3$  and passed through a short silica gel column to remove the non-porphyrinic components from the crude reaction mixture. This mixture was purified with a second column to afford the compound **FB-por** (yield: 3%).  $^1\text{H NMR}$  ( $\text{CDCl}_3$ )  $\delta$  (TMS, ppm): 8.95 (d, 2H), 8.69–8.73 (m, 6H), 8.43 (d, 2H), 8.30 (d, 2H), 8.07 (d, 2H), 7.39–7.45 (m, 10H), 7.13 (m, 2H), 4.10 (s, 3H), 2.64 (s, 6H), 1.84 (s, 12H), –2.59 (s, 2H); FT-IR (KBr pellet,  $\text{cm}^{-1}$ ): 1720 (ester, C=O), 3455 (amine, –NH).

#### 2.4.11. 5,15-Bis(2,4,6-trimethylphenyl)-15-{4-[Bis-[4-(2-ethylhexyloxy)-phenyl]-amino]}-(4-methoxycarbonylphenyl) porphyrin (**11**)

Compound **11** was synthesized by the same method as compound **9**.

$^1\text{H NMR}$  ( $\text{CDCl}_3$ )  $\delta$  (TMS, ppm): 8.96 (d, 2H), 8.67–8.72 (m, 6H), 8.42 (d, 2H), 8.30 (d, 2H), 7.98 (d, 2H), 7.28–7.35 (m, 6H), 6.95 (d, 4H), 4.10 (s, 3H), 3.88 (d, 4H), 1.77–1.81 (m, 2H), 1.20–1.54 (m, 16H), 0.86–0.98 (m, 12H), –2.57 (s, 2H); FT-IR (KBr pellet,  $\text{cm}^{-1}$ ): 1750 (ester, C=O), 3450 (amine, –NH).

#### 2.4.12. 5,15-Bis(2,4,6-trimethylphenyl)-15-triphenylamino(4-methoxycarbonylphenyl) porphyrinatozinc (**10**)

5,15-Bis(2,4,6-trimethylphenyl)-15-triphenylamino(4-methoxycarbonylphenyl) porphyrin (0.5 g, 0.54 mmol) and zinc acetate dehydrate (0.59 g, 2.71 mmol) were suspended in dry THF (20 ml). The mixture was then purged with  $\text{N}_2$  and slowly heated to  $80^\circ\text{C}$ .

It was then brought to reflux under  $\text{N}_2$  until there was no free base left as revealed by TLC (24 h). The mixture was then cooled to room temperature and the solvent was removed by vacuum distillation. The crude product left behind was then dried completely and purified with a column to afford the compound **Zn-por** (yield: 79%).  $^1\text{H NMR}$  ( $\text{CDCl}_3$ )  $\delta$  (TMS, ppm): 8.95 (d, 2H), 8.69–8.73 (m, 6H), 8.43 (d, 2H), 8.30 (d, 2H), 8.07 (d, 2H), 7.39–7.45 (m, 10H), 7.13 (m, 2H), 4.10 (s, 3H), 2.64 (s, 6H), 1.84 (s, 12H); FT-IR (KBr pellet,  $\text{cm}^{-1}$ ): 1720 (ester, C=O).

#### 2.4.13. 5,15-Bis(2,4,6-trimethylphenyl)-15-{4-[Bis-[4-(2-ethylhexyloxy)-phenyl]-amino]}-(4-methoxycarbonylphenyl) porphyrinatozinc (**12**)

Compound **12** was synthesized by the same method as compound **10**.

$^1\text{H NMR}$  ( $\text{CDCl}_3$ )  $\delta$  (TMS, ppm): 8.96 (d, 2H), 8.67–8.72 (m, 6H), 8.42 (d, 2H), 8.30 (d, 2H), 7.98 (d, 2H), 7.28–7.35 (m, 6H), 6.95 (d, 4H), 4.10 (s, 3H), 3.88 (d, 4H), 1.77–1.81 (m, 2H), 1.20–1.54 (m, 16H), 0.86–0.98 (m, 12H); FT-IR (KBr pellet,  $\text{cm}^{-1}$ ): 1750 (ester, C=O).

#### 2.4.14. 5,15-Bis(2,4,6-trimethylphenyl)-15-triphenylamino(4-carboxyphenyl) porphyrinatozinc (**HKK-Por 4**)

5,15-Bis(2,4,6-trimethylphenyl)-15-triphenylamino(4-methoxycarbonylphenyl) porphyrinatozinc (0.18 g, 0.18 mmol) and KOH (0.08 g, 0.14 mmol) were dissolved in THF-EtOH- $\text{H}_2\text{O}$  (1:1:0.1, 50 ml), and the solution was refluxed for 12 h. The mixture was then cooled to room temperature, acidified with concentrated HCl, and extracted with  $\text{CH}_2\text{Cl}_2$ . The organic phase was washed with sodium bicarbonate solution and water and dried with  $\text{Na}_2\text{SO}_4$ . The crude product left behind was then dried completely and purified with a column to afford the compound **Zn-por-COOH** (yield: 70%).  $^1\text{H NMR}$  ( $\text{CDCl}_3$ )  $\delta$  (TMS, ppm): 8.95 (d, 2H), 8.69–8.73 (m, 6H), 8.43 (d, 2H), 8.30 (d, 2H), 8.07 (d, 2H), 7.39–7.45 (m, 10H), 7.13 (m, 2H), 2.64 (s, 6H), 1.84 (s, 12H);  $\lambda_{\text{max,abs}}$  in THF: 426.5, 557.5, 599.5.  $\lambda_{\text{max,em}}$

**Table 1**  
Absorption/emission and electrochemical properties of **HKK-Por** dyes.

Dye	Absorption ( $\lambda_{\text{max}}/\text{nm}$ ) <sup>a</sup> ( $\epsilon/\text{M}^{-1}\text{cm}^{-1}$ )	Emission ( $\lambda_{\text{max}}/\text{nm}$ )	$E_{\text{ox}}^b/\text{V}$ (vs NHE)	$E_{\text{o-o}}^c/\text{V}$	$E_{\text{LUMO}}^d/\text{V}$ (vs NHE)
<b>HKK-Por 3</b>	424.5(340000), 554.5(12300), 598.5(8418)	608.9, 659.1	1.03	2.11	–1.08
<b>HKK-Por 4</b>	426.5(335000), 557.5(20493), 599.5(8524)	609.1, 660.0	1.05	2.10	–1.05
<b>HKK-Por 5</b>	425.5(365000), 558.0(18526), 601.0(8968)	612.0, 660.1	1.37	2.02	–0.65

<sup>a</sup> Absorption was measured in THF solution ( $1.0 \times 10^{-6}$  M) at room temperature.

<sup>b</sup> The oxidation potential of the dye on  $\text{TiO}_2$  was measured in acetonitrile with 0.1 M TBAPF<sub>6</sub> with a scan rate of  $50\text{ mV s}^{-1}$  (vs NHE).

<sup>c</sup>  $E_{\text{o-o}}$  was determined from the intersection of the absorption and emission spectra in THF.

<sup>d</sup> LUMO was calculated by  $E_{\text{ox}} - E_{\text{o-o}}$ .

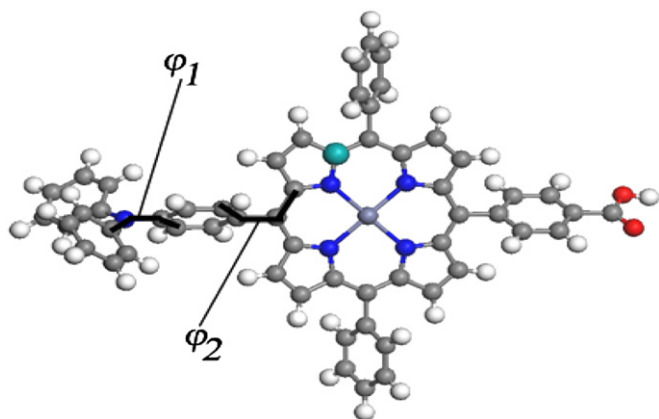


Fig. 3. Optimized structure of **HKK-Por 3** dye ( $\phi_1: \sim -37.7^\circ$ ;  $\phi_2: \sim -61.1^\circ$ ).

in THF: 609.1, 660.0; FT-IR (KBr pellet,  $\text{cm}^{-1}$ ): 2400–3400 (carboxylic acid,  $-\text{COOH}$ ); FAB-MS ( $m/z$ ): calcd. 973.3, found 973.0.

2.4.15. 5,15-Bis(2,4,6-trimethylphenyl)-15-{4-[Bis-[4-(2-ethylhexyloxy)-phenyl]-amino]}-(4-carboxylphenyl) porphyrinatozinc (**HKK-Por 5**)

**HKK-Por 5** was synthesized by the same method as **HKK-Por 4**.  $^1\text{H NMR}$  ( $\text{CDCl}_3$ )  $\delta$  (TMS, ppm): 8.96 (d, 2H), 8.67–8.72 (m, 6H), 8.42 (d, 2H), 8.30 (d, 2H), 7.98 (d, 2H), 7.28–7.35 (m, 6H), 6.95 (d, 4H), 3.88 (d, 4H), 1.77–1.81 (m, 2H), 1.20–1.54 (m, 16H), 0.86–0.98 (m, 12H);  $\lambda_{\text{max,abs}}$  in THF: 425.5, 558.0, 601.0.  $\lambda_{\text{max,em}}$  in THF: 612.0, 660.1; FT-IR (KBr pellet,  $\text{cm}^{-1}$ ): 2400–3500 (carboxylic acid,  $-\text{COOH}$ ); MS (MALDI-TOF): 1229.2 ( $\text{M}^+$ ).

2.5. Fabrication and testing of DSSC

FTO glass plates (Pilkington) were cleaned in a detergent solution using an ultrasonic bath for 1 h and rinsed with water and ethanol. The FTO glass plates were immersed in an aqueous solution of 40 mM  $\text{TiCl}_4$  at  $70^\circ\text{C}$  for 30 min and washed with water and ethanol. The first  $\text{TiO}_2$  layer of 8  $\mu\text{m}$  thickness was prepared by screen printing  $\text{TiO}_2$  paste (Solaronix, 13 nm anatase), and the second scattering layer containing 400 nm sized anatase particles was deposited by screen printing. The  $\text{TiO}_2$  electrodes were immersed into the dye solution [0.3 mM in ethanol/THF (1:1) with DCA (40 mM)] and kept at room temperature overnight. Counter electrodes were prepared by coating with a drop of  $\text{H}_2\text{PtCl}_6$  solution (2 mg of Pt in 1 mL of ethanol) on an FTO plate. The dye-adsorbed  $\text{TiO}_2$  electrode and Pt-counter electrode were assembled into a sealed sandwich-type cell. A drop of the electrolyte, which was composed of 0.6 M 1,2-dimethyl-3-propyl imidazolium iodide,

0.05 M iodine, 0.1 M LiI, and 0.5 M tert-butylpyridine in acetonitrile, was then introduced into the cell. It was introduced into the inter-electrode space from the counter electrode side through predrilled holes. The drilled holes were sealed with a microscope cover slide and Surllyn to avoid leakage of the electrolyte solution.

2.6. Photoelectrochemical measurements of DSSCs

Photoelectrochemical data were measured using a 1000 W xenon light source (Oriel, 91193) that was focused to give  $1000 \text{ W/m}^2$ , the equivalent of one sun at Air Mass (AM) 1.5, at the surface of the test cell. The light intensity was adjusted with a Si solar cell that was double-checked with an NREL-calibrated Si solar cell (PV Measurement Inc.). The applied potential and measured cell current were measured using a Keithley model 2400 digital source meter. The current–voltage characteristics of the cell under these conditions were determined by biasing the cell externally and measuring the generated photocurrent. This process was fully automated using Wavemetrics software.

3. Results and discussion

The novel zinc porphyrins were synthesized according to Scheme 1. Compounds **1–6** were prepared by adapting published procedures [30,34]. Compound **7** was synthesized according to the literature [35]. Compound **8** was synthesized by an insertion reaction of Zn(II) ions and then hydrolysed (**HKK-Por 3**). **HKK-Por 4** and **HKK-Por 5** dyes were synthesized by the same method.

Fig. 1 shows the absorption and emission spectra of **HKK-Por** dyes measured in THF solution; their photophysical properties are summarized in Table 1. The absorption spectrum of **HKK-Por 3** displays three absorption maxima at 424.5 nm, 554.5 nm, and 598.5 nm, which are assigned as the  $\pi-\pi^*$  transitions of the conjugated system. **HKK-Por 4** and **HKK-Por 5** also have similar behaviour to **HKK-Por 3**. In contrast, the absorption spectra of **HKK-Por** dyes adsorbed on the  $\text{TiO}_2$  surface are remarkably broadened relative to the absorption spectra of the solution state (Fig. 2). This might be due to dye–dye and/or dye– $\text{TiO}_2$  interactions [36,37]. A large red-shift of the absorption maxima due to introduction of the TPA moiety was expected in the D- $\pi$ -A porphyrins, but **HKK-Por** dyes were a little red-shifted in contrast to Zn[5,10,15-triphenyl-20-(4-carboxylphenyl)-porphyrin], due to the tilted structure ( $\phi_1: \sim -37.7^\circ$ ,  $\phi_2 \sim -61.1^\circ$ ) between TPA and the porphyrin unit, as shown in Fig. 3. In order to find out which molecular transitions in our dyes are responsible for the electron transport in our DSSC, we have made a detailed analysis of the TD-DFT results. Table-S1 summarizes absorption peaks and major contributions to each of them. Evidently, the most efficient electron transport in the DSSCs will be contributed by the charge transfer

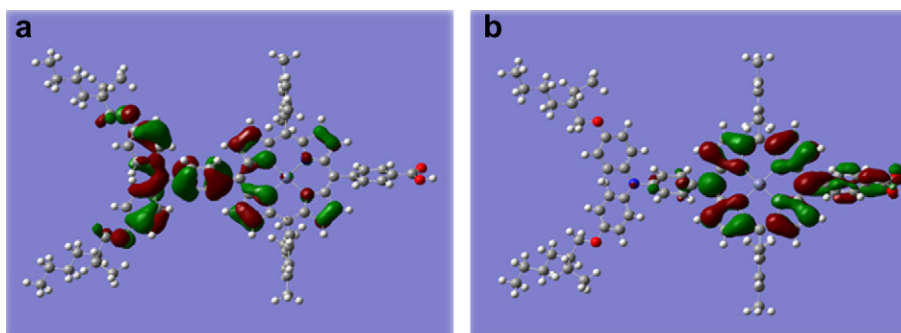
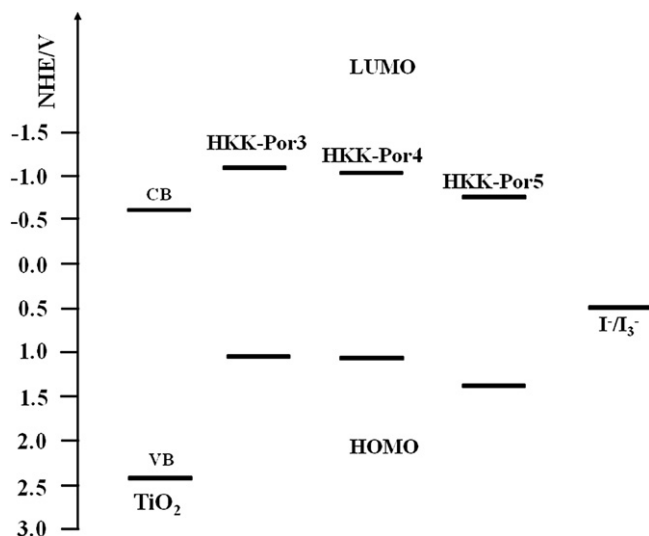


Fig. 4. Plots of the isodensity surfaces (PBE/PBE/6-31G\*) of HOMO-12 and LUMO of **HKK-Por 5** dye.



**Fig. 5.** Overview of the evaluated energy levels of **HKK-Por** dyes determined by cyclic voltammetry.

transition from the donor to the acceptor. In fact, the table shows that the transition from HOMO-12 to LUMO exclusively corresponds to the charge transfer transition among all transitions. The transition makes a big contribution to the absorption of **HKK-Por 5**, which peaked at 425.5 nm in Fig. 1, as indicated by the large oscillation strengths of transitions at 400 and 414 nm in Table-S1. Our analysis indicates that the HOMO-12 of **HKK-Por 5** is raised by 0.35 eV with respect to the corresponding MO (= HOMO-11) of **HKK-Por 4**, while LUMO levels of the two dyes are located almost at the same energy level. Therefore, the HOMO-11 to LUMO transition of **HKK-Por 4**, which corresponds to the UV region, is red-shifted to 400 and 414 nm by the electron-donating group of **HKK-Por 5**, as shown in Table 1. The electrochemical properties were investigated by cyclic voltammetry (CV) to obtain the HOMO and LUMO levels of the **HKK-Por** dyes. The cyclic voltammogram curves were obtained from a three-electrode cell in 0.1 M TBAPF<sub>6</sub> in CH<sub>3</sub>CN at a scan rate of 50 mV/s, using a dye-coated TiO<sub>2</sub> electrode as a working electrode, a Pt wire counter electrode, and an Ag/AgCl (saturated KCl) reference electrode (+0.197 V vs NHE) and calibrated with ferrocene. All of the measured potentials were converted to the NHE scale. The LUMOs of the **HKK-Por 3**, **HKK-Por 4**, and **HKK-Por 5** estimated from the oxidation potential and the energy at the intersection point of absorption and emission spectra are 1.03 V, 1.05 V, and 1.37 V vs NHE, respectively. In addition, with the introduction of the bulky stronger donor group, the energy levels of HOMO and LUMO are largely changed. **HKK-Por 5** dye has a HOMO level of 1.37 V (vs NHE) and a LUMO level of -0.65 V (vs NHE) (Fig. 4). HOMO values of **HKK-Por** dyes (1.03–1.37 V vs NHE) were more positive than the I<sup>-</sup>/I<sub>3</sub><sup>-</sup> redox couple (0.4 V vs NHE) so effective dye regeneration could be possible (Fig. 5). The electron injection from the excited sensitizers to the conduction band of TiO<sub>2</sub> should be energetically favourable because of the more negative LUMO

**Table 2**  
Dye-sensitized solar cell performance data of the **HKK-Por** dyes.

Dye	$J_{sc}$ (mA/cm <sup>2</sup> )	$V_{oc}$ (V)	FF	$\eta$ (%)
<b>HKK-Por 3</b>	5.38	0.59	0.66	2.09
<b>HKK-Por 4</b>	7.57	0.54	0.67	2.74
<b>HKK-Por 5</b>	9.04	0.57	0.66	3.36

TiO<sub>2</sub> thickness 9.5 + 4, sc, TiCl<sub>4</sub>; electrolyte condition 0.6 M DMP11, 0.5 M LiI, 0.05 M I<sub>2</sub>, 0.5 M TBP in an acetonitrile solution; dye was dissolved in THF.

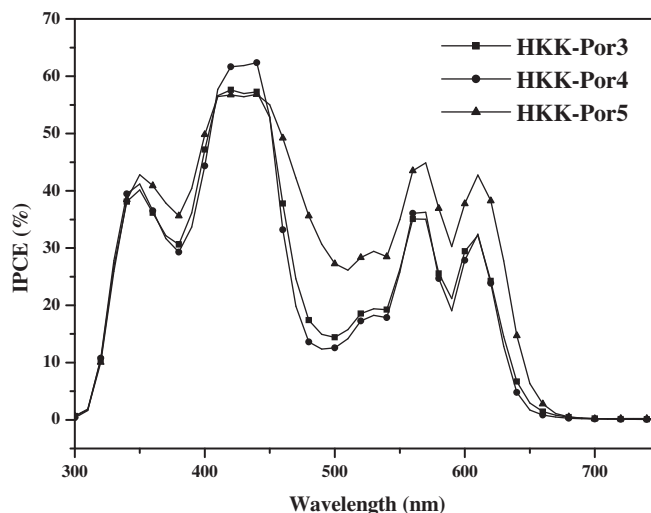


**Fig. 6.** Typical action spectra of incident photon-to-current conversion efficiencies (IPCEs) obtained for nanocrystalline TiO<sub>2</sub> solar cells sensitized by **HKK-Por** dyes.

values (-0.65 to -1.08 vs NHE) compared to the conduction band edge energy level of the TiO<sub>2</sub> electrode [38].

The photovoltaic properties of the solar cells constructed from these organic dye-sensitized TiO<sub>2</sub> electrodes were measured under simulated AM1.5 irradiation (100 mW/cm<sup>2</sup>). The photovoltaic performances of the **HKK-Por**-DSSCs are summarized in Table 2. Incident photon-to-current conversion efficiencies (IPCEs) and current density-voltage (J-V) characteristics of devices are shown in Figs. 6 and 7, respectively.

The onset wavelengths of the IPCE spectra for DSSCs based on **HKK-Por** dyes were <700 nm. IPCE values higher than 70% were observed in the range of 400–500 nm. The maximum IPCE value of the DSSC based on **HKK-Por 5** was slightly higher than the efficiencies of the DSSCs based on other **HKK-Por** dyes due to the introduction of the alkoxy group into the TPA moiety. Under standard global AM 1.5 solar conditions, the **HKK-Por 5** sensitized cell gave a  $J_{sc}$  of 9.04 mA cm<sup>-2</sup>,  $V_{oc}$  of 0.57 V, and FF of 0.66, corresponding to an overall conversion efficiency of 3.36%. The introduction of a bulky alkoxy group into the TPA donor unit gives a strong donating effect and reducing the aggregation of dyes.

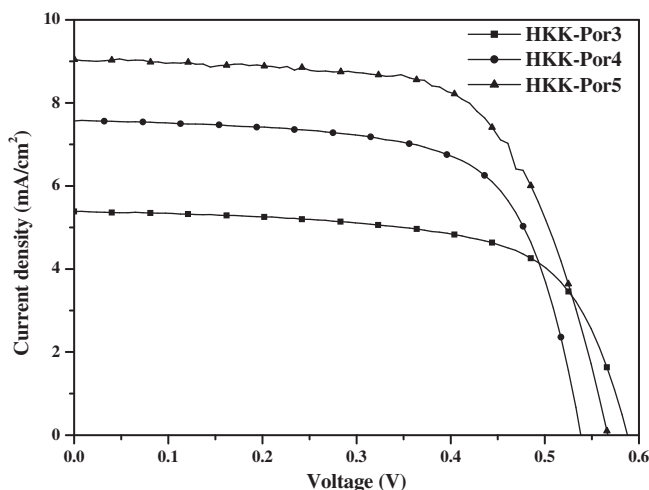


**Fig. 7.** Photocurrent–voltage characteristics of representative TiO<sub>2</sub> electrodes sensitized with **HKK-Por** dyes.

Also, the introduction of the bulky alkoxy substituent into the TPA moiety at the meso position of the porphyrin ring could lead to a fast dye-regeneration in order to avoid the geminate charge recombination between oxidized sensitizers and photoinjected electrons in the nanocrystalline TiO<sub>2</sub> film, thus enhancing the **HKK-Por 5** sensitized cell performance.

#### 4. Conclusions

We have successfully synthesized a novel D- $\pi$ -A system based on zinc porphyrin dyes and obtained materials with interesting optical and electrochemical properties. Under standard global AM 1.5 solar conditions, the **HKK-Por 5** sensitizer cell gave a  $J_{SC}$  of 9.04 mA cm<sup>-2</sup>,  $V_{OC}$  of 0.57 V, and FF of 0.66, corresponding to an overall conversion efficiency of 3.36%. Because of a bulky donor effect, HKK-Por dyes with an alkoxy-containing TPA moiety showed a higher conversion efficiency. Further improvement of the power conversion efficiency of porphyrin derivative dyes can be investigated by using them as dye sensitizers instead of expensive ruthenium dye sensitizers in the near future.

#### Acknowledgements

This research was supported by MKE (the Ministry of Knowledge Economy), Korea, under the ITRC support programme supervised by the IITA (Institute for Information Technology Advancement) (IITA-2008-C1090-0804-0013), the WCU (the Ministry of Education and Science) programme (R31-2008-000-10035-0), and the CRC Program through the National Research Foundation of Korea (NRF) (2010K000973). Computations were performed using a supercomputer at the Korea Institute of Science and Technology Information (KSC-2011-C1-11).

#### Appendix. Supplementary material

Supplementary data associated with this article can be found, in the online version, at doi:10.1016/j.dyepig.2011.12.006.

#### References

- Grätzel M. Photoelectrochemical cells. *Nature* 2001;414:338–44.
- Nazeeruddin MK, De Angelis F, Fantacci S, Selloni A, Viscardi G, Grätzel M, et al. Combined experimental and DFT-TDDFT computational study of photoelectrochemical cell ruthenium sensitizers. *J Am Chem Soc* 2005;127:16835–47.
- Nazeeruddin MK, Péchy P, Renouard T, Zakeeruddin SM, Humphry-Baker R, Grätzel M, et al. Engineering of efficient panchromatic sensitizers for nanocrystalline TiO<sub>2</sub>-based solar cells. *J Am Chem Soc* 2001;123:1613–24.
- Mishra A, Fischer MKR, Bäuerle P. Metal-free organic dyes for dye-sensitized solar cells: from structure: property relationships to design rules. *Angew Chem Int Ed* 2009;48:2474–99.
- Ning Z, Fu Y, Tian H. Improvement of dye-sensitized solar cells: what we know and what we need to know. *Energy Environ Sci* 2010;3:1170–81.
- Baek NS, Yum JH, Zhang X, Kim HK, Nazeeruddin MK, Grätzel M. Functionalized alkyne bridged dendron based chromophores for dye-sensitized solar cell applications. *Energy Environ Sci* 2009;2:1082–7.
- Seo KD, Song HM, Lee MJ, Nazeeruddin MK, Grätzel M, Kim HK, et al. Coumarin dyes containing low-band-gap chromophores for dye-sensitized solar cells. *Dyes Pigment* 2011;90:304–10.
- Wu W, Xu X, Yang H, Hua J, Zhang X, Tian H, et al. D- $\pi$ -M- $\pi$ -A structured platinum acetylide sensitizer for dye-sensitized solar cells. *J Mater Chem* 2011;21:10666–71.
- Ning Z, Tian H. Triarylamine: a promising core unit for efficient photovoltaic materials. *Chem Commun*; 2009:5483–95.
- Zhu W, Wu Y, Wang S, Li W, Wang Z, Tian H, et al. Organic D-A- $\pi$ -A solar cell sensitizers with improved stability and spectral response. *Adv Funct Mater* 2011;21:756–63.
- Liang Y, Peng B, Liang J, Tao Z, Chen J. Triphenylamine-based dyes bearing functionalized 3,4-propylenedioxythiophene linkers with enhanced performance for dye-sensitized solar cells. *Org Lett* 2010;12:1204–7.
- Velusamy M, Thomas KRJ, Lin JT, Hsu YC, Ho KC. Organic dyes incorporating low-band-gap chromophores for dye-sensitized solar cells. *Org Lett* 2005;7:1899–902.
- Gouterman M. Spectra of porphyrins. *J Mol Spectrosc* 1961;6:138–63.
- Mozer AJ, Griffith MJ, Tsekouras G, Wagner P, Wallace GG, Officer DL, et al. Zn–Zn porphyrin dimer-sensitized solar cells: toward 3-D light harvesting. *J Am Chem Soc* 2009;131:15621–3.
- Park JK, Lee HR, Chen J, Shinokubo H, Osuka A, Kim D. Photoelectrochemical properties of doubly  $\beta$ -functionalized porphyrin sensitizers for dye-sensitized nanocrystalline-TiO<sub>2</sub> solar cells. *J Phys Chem C* 2008;112:16691–9.
- Cherian S, Wamser CC. Adsorption and photoactivity of tetra(4-carboxyphenyl)porphyrin (TCPP) on nanoparticulate TiO<sub>2</sub>. *J Phys Chem B* 2000;104:3624–9.
- Watson DF, Marton A, Stux AM, Meyer GJ. Insights into dye-sensitization of planar TiO<sub>2</sub>: evidence for involvement of a protonated surface state. *J Phys Chem B* 2003;107:10971–3.
- Watson DF, Marton A, Stux AM, Meyer GJ. Influence of surface protonation on the sensitization efficiency of porphyrin-derivatized TiO<sub>2</sub>. *J Phys Chem B* 2004;108:11680–8.
- Rochford J, Chu D, Hagfeldt A, Galoppini E. Tetrachelate porphyrin chromophores for metal oxide semiconductor sensitization: effect of the spacer length and anchoring group position. *J Am Chem Soc* 2007;129:4655–65.
- Rochford J, Galoppini E. Zinc(II) tetraarylporphyrins anchored to TiO<sub>2</sub>, ZnO, and ZrO<sub>2</sub> nanoparticle films through rigid-rod linkers. *Langmuir* 2008;24:5366–74.
- Martínez-Díaz MV, Torre GDL, Torres T. Lighting porphyrins and phthalocyanines for molecular photovoltaics. *Chem Commun* 2010;46:7090–108.
- Imahori H, Umeyama T, Ito S. Large  $\pi$ -aromatic molecules as potential sensitizers for highly efficient dye-sensitized solar cells. *Acc Chem Res* 2009;42:1809–18.
- Walter MG, Rudine AB, Wamser CC. Porphyrins and phthalocyanines in solar photovoltaic cells. *J Porphyrins Phthalocyanines* 2010;14:759–92.
- Liu Y, Lin H, Dy JT, Tamaki K, Nakazaki J, Segawa H, et al. *N*-fused carbazole–zinc porphyrin–free-base porphyrin triad for efficient near-IR dye-sensitized solar cells. *Chem Commun* 2011;47:4010–2.
- Imahori H, Matsubara Y, Iijima H, Umeyama T, Matano Y, Ito S, et al. Effects of meso-diarylamino group of porphyrins as sensitizers in dye-sensitized solar cells on optical, electrochemical, and photovoltaic properties. *J Phys Chem C* 2010;114:10656–65.
- Eu S, Hayashi S, Umeyama T, Oguro A, Kawasaki M, Imahori H, et al. Effects of 5-membered heteroaromatic spacers on structures of porphyrin films and photovoltaic properties of porphyrin-sensitized TiO<sub>2</sub> cells. *J Phys Chem C* 2007;111:3528–37.
- Lee CW, Lu HP, Lan CM, Huang YL, Diao EWG, Yeh CY, et al. Novel zinc porphyrin sensitizers for dye-sensitized solar cells: synthesis and spectral, electrochemical, and photovoltaic properties. *Chem Eur J* 2009;15:1403–12.
- Mathew S, Iijima H, Toude Y, Umeyama T, Matano Y, Imahori H, et al. Optical, electrochemical, and photovoltaic effects of an electron-withdrawing tetrafluorophenylene bridge in a push-pull porphyrin sensitizer used for dye-sensitized solar cells. *J Phys Chem C* 2011;115:14415–24.
- Chang YC, Wang CL, Pan TY, Hong SH, Lin CY, Diao EWG, et al. A strategy to design highly efficient porphyrin sensitizers for dye-sensitized solar cells. *Chem Commun* 2011;47:4010–2.
- Lee MJ, Seo KD, Song HM, Kang MS, Kang HS, Kim HK, et al. Novel D- $\pi$ -A system based on zinc-porphyrin derivatives for highly efficient dye-sensitized solar cells. *Tetrahedron Lett* 2011;52:3879–82.
- Kresse G, Hafner J. Ab initio molecular dynamics for liquid metals. *Phys Rev B* 1993;47:558–61.
- Kresse G, Furthmüller J. Efficient iterative schemes for ab initio total-energy calculations using a plane-wave basis set. *Phys Rev B* 1996;54:11169–86.
- Frisch MJ, Trucks GW, Schlegel HB, Scuseria GE, Robb MA, Cheeseman JR, et al. Gaussian03, Revision B.05. Pittsburgh PA: Gaussian, Inc.; 2003.
- Lee DH, Lee MJ, Song HM, Song BJ, Seo KD, Kim HK, et al. Organic dyes incorporating low-band-gap chromophores based on  $\pi$ -extended benzothiadiazole for dye-sensitized solar cells. *Dyes Pigment* 2011;91:192–8.
- Kang MS, Oh JB, Seo KD, Roh SG, Kim HK, Pakt NG, et al. Novel extended  $\pi$ -conjugated Zn(II)-porphyrin derivatives bearing pendant triphenylamine moiety for dye-sensitized solar cell: synthesis and characterization. *J Porphyrins Phthalocyanines* 2009;13:798–804.
- Kasha M. Energy transfer mechanisms and the molecular exciton model for molecular aggregates. *Radiat Res* 1963;20:55–70.
- Lin CY, Lo CF, Luo L, Lu HP, Hung CS, Diao EWG. Design and characterization of novel porphyrins with oligo(phenylethynyl) links of varied length for dye-sensitized solar cells: synthesis and optical, electrochemical, and photovoltaic investigation. *J Phys Chem C* 2009;113:755–64.
- Hagfeldt A, Grätzel M. Light-induced redox reactions in nanocrystalline systems. *Chem Rev* 1995;95:49–68.